Physica B: Condensed Matter 546 (2018) 67–72

Contents lists available at ScienceDirect

Physica B: Condensed Matter

journal homepage: www.elsevier.com/locate/physb

On the optical and magnetic studies of $YCrO_3$ perovskites

Antonio N.L. Jara[a,b], Jesiel F. Carvalho[a], Adolfo Franco Júnior[a], Lauro J.Q. Maia[a], Ricardo C. Santana[a,*]

[a] Instituto de Física, Universidade Federal de Goiás, Av. Esperança, Campus Samambaia, 74690-900 Goiânia (GO), Brazil
[b] Universidad Nacional de Ingeniería, Peru

ARTICLE INFO

Keywords:
Orthochromite
$YCrO_3$
Modified polymeric precursor method
EPR
Magnetic transition

ABSTRACT

In this paper we studied the Electron Paramagnetic Resonance (EPR) and Optical spectroscopies of mono disperse yttrium chromite ($YCrO_3$) nanoparticles prepared by a modified polymeric precursor method. The particles crystallized in roughly spherical shape with size ranging from 100 to 200 nm. Diffuse reflectance spectrum exhibited very well defined bands related to the $^4A_2 \rightarrow {}^4T_2$, $^4A_2 \rightarrow {}^4T_1$, $^4A_2 \rightarrow {}^2T_1$, $^4A_2 \rightarrow {}^2E$ transitions, characteristic of Cr^{3+} ($3d^3$, $^2D_{5/2}$) ions in nearly octahedral symmetry. The crystalline field *Dq*, Racah parameters (*B* and *C*) and *Dq/B*, could be determined and the results indicated that Cr^{3+} ions are in a strong ligand field site. The EPR spectra of $YCrO_3$ shows a single broad resonance in the whole range of temperature studied, 100–300 K. Combining optical and EPR results the effective *g*-values of the paramagnetic Cr^{3+} were estimated to be 1.97 and 1.98, respectively, typical of Cr^{3+} in orthorhombic crystal field environment. The onset of the antiferro-paramagnetic transition, $T_{\tilde{N}}$140 K, attributed to Cr^{3+}-Cr^{3+} exchange interaction ($J = -41.5\,cm^{-1}$) was determinate by means of Magnetization and EPR measurements. The results were discussed in terms of the magnetic short-rang spin-spin exchange interaction between pairs of Cr^{3+}.

1. Introduction

Yttrium chromite ($YCrO_3$) material exhibits interesting physical properties, principally the coexistence of magnetic and ferroelectric properties that allow its applications in spintronic, optoelectronic, thermistors among others [1,2], being one of the most investigated bifferoic materials at room temperature. However, the understanding of the origin of the magnetic properties requires additional studies to elucidate its relations to the crystal structure, which seems to be depended on the synthesis methods. Among widely used synthesis method to prepare $YCrO_3$ crystalline structure, combustion reaction [11–13], sol-gel [14,15], hydrothermal synthesis [16], and conventional solid-state reaction [3] have being the most used.

Looby and Katz [3] reported that the $YCrO_3$ crystalline structure as monoclinic, but subsequently Katz [4] suggested the possibility of an orthorhombic structure. Latter on this was confirmed by the work of Geller and Wood [5], which $YCrO_3$ crystallizes in a centrosymmetric perovskite orthorhombic structure with space group P*bnm*. Nevertheless, recently Serrao et al. [6] reported that $YCrO_3$ was weakly ferroelectric below 473 K. Using high-resolution neutron diffraction Ramesha et al. [7] determined the $YCrO_3$ crystal structure confirming the centrosymmetric perovskite structure with space group *Pnma* and relating the ferroelectric behavior to a local noncentrosymmetry due to dislocation of Cr ions by about 0.01 Å in the *z* direction.

According to Judin et al. [8] magnetism studies single crystals of $YCrO_3$ is antiferromagnetic, presenting a weak ferromagnetism below $T_N = 141$ K. The ferromagnetism was attributed to canted antiferromagnetism combined with the ferroelectricity associated to the local noncentrosymmetry around chromium ions, although to be weak effects, turning yttrium chromite an interesting bifferoic material from the scientific point of view. Thus, it motivated us to study the magnetic properties of $YCrO_3$ nanoparticles by means of Electron Paramagnetic Resonance (EPR) spectroscopy. It is well known that EPR is one of the most sensitive techniques for detecting the influence of local structure on paramagnetic ions, and temperature magnetic phase transitions.

To the best of our knowledge the EPR studies of $YCrO_3$ in regard of the method of preparation with the optical and magnetic properties are scarce in the literature [9,10]. So, the magneto-optical properties of $YCrO_3$ were deeply studied by optical and EPR spectroscopies.

In this work, we used a modified polymeric precursor method, described in detail in Ref. [17] to synthesize $YCrO_3$ powders. This method has been proved to be efficiently to synthesis particles with good crystallinity, chemically homogeneous [17].

* Corresponding author.
E-mail addresses: tony2530@hotmail.com (A.N.L. Jara), santana@ufg.br (R.C. Santana).

https://doi.org/10.1016/j.physb.2018.07.026
Received 20 June 2018; Received in revised form 13 July 2018; Accepted 25 July 2018
Available online 29 July 2018
0921-4526/

2. Experimental section

2.1. Synthesis of the compounds

Polycrystalline $YCrO_3$ powder was synthesized by a modified polymeric precursor method, which was successful applied to the synthesis of $YAlO_3$ and whose details are described in Ref. [17]. Stoichiometric quantities of yttrium nitrate, $Y(NO_3)_3{\cdot}6H_2O$ (Acros Organics Co., 99.9%) and chromium nitrate $Cr(NO_3)_3{\cdot}9H_2O$ (Acros Organics Co., 99.9%) were completely dissolved in water with citric acid in 3:1 M ratio of acid to metal. Separately D-sorbitol was also water dissolved in the molar ratio of 3:2 (citric acid/D-sorbitol). Both solutions were merged in a single vessel and stirred at 80 °C, during about 12 h, to remove the water excess and to complete the chemical reactions. The product was a homogeneous and stable gel with violet coloration. The gel was dried at 250 °C for 1 h using a heating rate of 0.5 °C/min, producing a dark brown porous material. After crushed, the dried powder was submitted to an additional pyrolytic thermal treatment at 700 °C for 12 h, under N_2 flux, to remove the excess of additives, avoiding uncontrolled firing. This procedure yielded black amorphous particles having irregular shapes, which were grinded to obtain a very fine powder using a ball mill with yttria stabilized zirconia spheres. The last stage was the calcination of this black powder by fast heating at 1300°C for 3 h, producing single-phase $YCrO_3$ powders having good crystallinity.

2.2. Characterization

X-ray diffraction (XRD) powder pattern was measured in a Shimadzu XRD 6000 diffractometer using CuKα (λ = 1.54056 Å) radiation, 0.02° step scan, time counting of 5 s, and a scintillator detector. The diffractogram was analyzed using the TOPAS software, from Bruker AXS. Images of scanning electron microscopy (SEM) were acquired using a microscope JEOL JSM–6610. Fourier transform infrared (FT-IR) spectra were measured in the range from 400 to 800 cm^{-1} using a PerkinElmer spectrophotometer, with samples diluted in 1.0% KBr pellets. Diffuse reflectance spectrum was obtained in a Perkin Elmer Lambda WB1050 spectrophotometer using a Praying Mantis diffuse reflection accessory.

EPR measurements were performed in an ESP-300 and EMX-1572 Bruker spectrometers working at 9.4 GHz (X-band), with standard Bruker rectangular cavities operating with of 100 kHz magnetic field modulation and ~5 mW microwave power. The frequency was measured with a Hewlett Packard 5350B microwave counter, the temperature was controlled by a Eurotherm nitrogen flow system with accuracy of ± 0.5 K. Magnetic external field could be varied from 10 to 810 mT. The line width, resonance field and intensity were obtained by simulations of each collected spectra with a derivative Lorentzian function and *g*-factor was calculated by the resonance condition equation $g = h\nu/\mu_B B_0$, where h is the Planck constant, ν is the microwave frequency, μ_B is the Bohr magneton and B_0 is the resonance magnetic field. Accuracy of measurement is 0.3 mT for resonance field, 0.5 mT for line width and 10% for intensity, obtained from spectra simulations. Measurements of magnetic susceptibility versus temperature were performed in a commercial superconducting quantum interference device (SQUID) magnetometer over the temperature range of 2–300 K.

3. Results and discussions

3.1. Structural characterization

Fig. 1 shows the measured and calculated, by Rietveld refinement, XRD patterns of synthesized $YCrO_3$ powders. The starting structural model used in the Rietveld refinement was that proposed by Ramesha et al. [7]. Careful refinement procedures demonstrated that this choice provides better convergence than the previous model of Ref. [3]. Our results (R_{wp} of 8%) show a single phase perovskite structure with space group *Pnma* and cell parameters a = 5.5181(4) Å, b = 7.5293(5) Å, c = 5.2389(4) Å and V = 217.66(5) $Å^3$, and the refined atomic coordinations are in good agreement with those in Ref. [8], this confirms that $YCrO_3$ belongs to the *Pnma* group.

The FTIR spectrum of $YCrO_3$ powder is shown in Fig. 2. The more prominent bands (see inset in Fig. 2) are the strong one at ~586 cm^{-1}, that can be assigned to the Cr-O stretching mode ($\nu_{Cr\text{-}O,str}$, 1), the band at 491 cm^{-1}, assigned to the Y-O stretching ($\nu_{Y\text{-}O,str}$, 2), and that at 443 cm^{-1} corresponding to the O-Cr-O deformation ($\nu_{O\text{-}Cr\text{-}O,def}$, 3) [18,19]. The band at 640 cm^{-1} and the shoulders at 570 and 512 cm^{-1} can be assigned to overtones of Cr-O vibration ($\nu_{Cr\text{-}O,vib}$, 4), while the band at 1385 cm^{-1} can be assigned to the stretching of NO_3^- (5) [15].

Fig. 3 shows a Scanning Electron Microscopy (SEM) image of dispersed $YCrO_3$ particles. The particles sizes lie in the range 100–200 nm, roughly spherical and uniformly distributed. Notice the presence of moderated coalescencent grains, as indicated by the arrows in Fig. 3.

3.2. Optical studies

The diffuse reflectance spectrum of $YCrO_3$ is shown in Fig. 4. It is evident the features of optical spectra of Cr^{3+} ions in a distorted octahedral local symmetry in orthochromites [20,21]. The spectrum shows two intense characteristic bands centered at ~604 nm and ~450 nm (~16,566 cm^{-1} and ~22,222 cm^{-1}) due the DMSO-d_6 transitions $^4A_2 \rightarrow {}^4T_2$ (parity-forbidden) and $^4A_2 \rightarrow {}^4T_1$ (spin-allowed), respectively. The $^4A_2 \rightarrow {}^2T_2$ appear as a shoulder at ~689 nm (14,514 cm^{-1}). The weak bands observed in the infrared region at ~733 nm and ~691 nm (13,643 cm^{-1} and 14,472 cm^{-1}) are due the $^4A_2 \rightarrow {}^2E$ and $^4A_2 \rightarrow {}^2T_1$ electronic transitions, respectively, that acquires spin-allowed character via spin-orbit interaction with the band $^4A_2 \rightarrow {}^4T_2$. The band at ~360 nm in ultraviolet region has been assigned to the charge transfer transition from *2p* valence of oxygen atoms to the 3d conduction band of Cr^{3+} ions [21].

From the energies of the ^2E, $^4T_2$ and $^4T_1$ excited states and the relations given by Casalboni et al. [21] and Rasheed et al. [22], are

$$10Dq = [E(^4A_2) - E(^4T_2)], \quad (1)$$

with

$$Dq/B = 15(x - 8)/(x^2 - 10x), \quad (2)$$

where

$$x = [E(^4A_2 \rightarrow {}^4T_1) - E(^4A_2 \rightarrow {}^4T_2)]/Dq, \quad (3)$$

and

$$C/B = (1/3.05)\{[E(^4A_2 \rightarrow {}^2E)/3.05] - 7.9 + 1.8(B/Dq)\}, \quad (4)$$

where B and C are the Racah parameters. B is a measure of the intensity of the inter-electronic repulsion in the 3d shell of the Cr^{3+} ions. Thus, the crystal field strength (Dq) parameters can be calculated. The obtained results are $10Dq$ = 16,566.29 cm^{-1}, Dq/B = 3.05, B = 542.88 cm^{-1} and C = 2962.25 cm^{-1}. Concerning the Dq/B parameter, the present value of 3.05, is consistent with the Cr^{3+} ions occupying a site with high crystalline field strength [21], and is in region close to the intersection between $^4T_2$ and $^2T_2$ levels being called high crystalline field. The crystal field theory [21] also predicts that small values of B results in more delocalized electrons on the Cr^{3+} ion taking as a consequence a decrease on the inter-electronic repulsion in the 3d shell and leading to a more covalent character between the oxygen and chromium ions. The B value found in this work for $YCrO_3$ prepared by the modified polymeric precursor method, presents similar values to those for lanthanide $LnCrO_3$ perovskites (Ln = Ho, Dy, Yb, Gd, Sm, Nd, La, Lu) [18], B lies in the range of 494–538 cm^{-1}. This result is consistent with the similar electronegativity of the Y and the Ln ions.

The nephelauxetic ratio, a measure of the decrease of the Racah B parameter when a transition metal ion forms a complex with ligand,

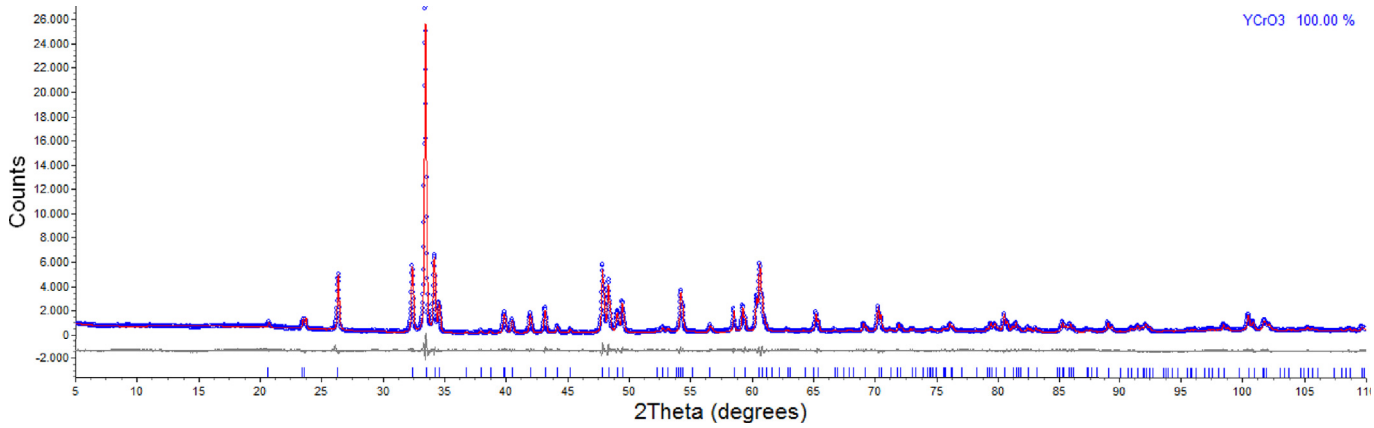

Fig. 1. X-ray powder diffraction of $YCrO_3$ with Rietveld refining. The blue points and red line indicate the measured and calculated diffractograms. The gray line below indicates the diffractogram difference and the vertical ticks the Bragg angles. (For interpretation of the references to color in this figure legend, the reader is referred to the Web version of this article.)

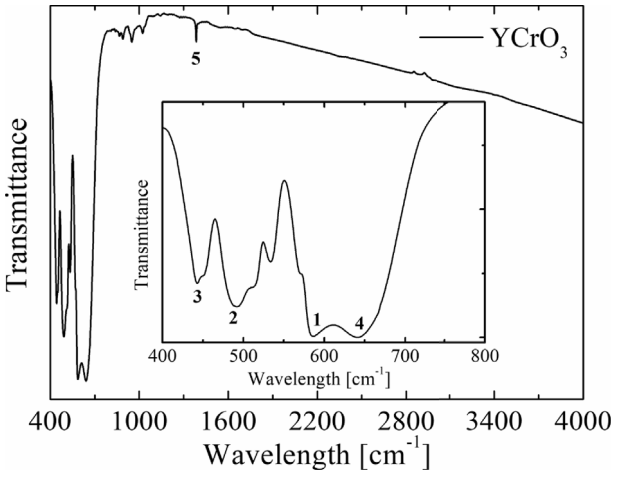

Fig. 2. Normalized FTIR spectrum of $YCrO_3$ taken at room temperature in the 400 to 4000 cm^{-1}. The inset shows details of the $YCrO_3$ IR bands, and the numbers denotes these principal bands as described in text.

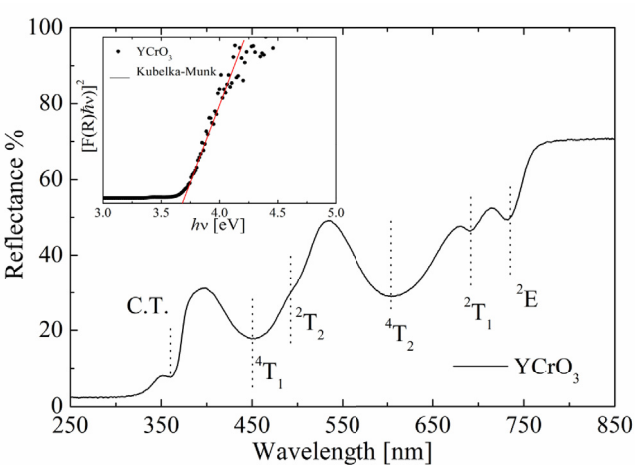

Fig. 4. Powder diffuse reflectance spectrum of $YCrO_3$ sample, taken at room temperature. Vertical dotted lines indicate the positions of observed bands. Inset shows the optical band gap determination using the Kubelka-Munk theory.

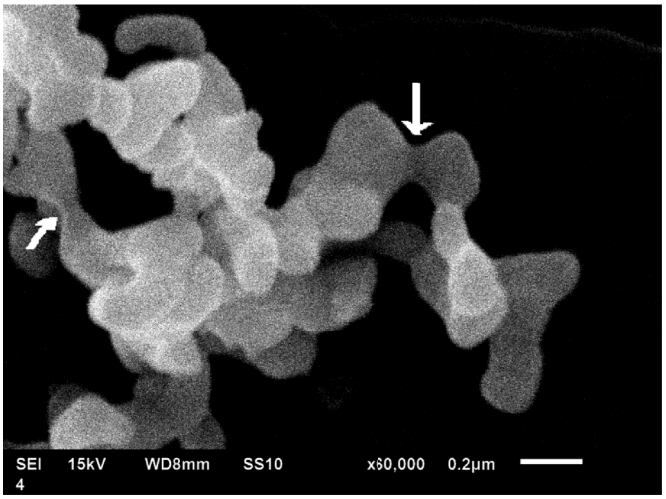

Fig. 3. Typical SEM image of perovskyteYCrO3 powder prepared by polymeric precursor method. A scale bar in the left bottom corner is 0.2 µm.

$\beta = 0.59$ ($\beta = B/B_0$, where B_0 is the Racah parameter for free ion, 918 cm^{-1}) is slightly larger than that obtained for Cr_2O_3 ($\beta = 0.52$) [23]. This is an indication that Cr-O linkage is less covalent in $YCrO_3$ chromite, in good agreement with those reported for Cr^{3+} ions in $YCrO_3$ nanopowders [12,13]. Furthermore, the higher covalency of Y-O linkage could be an important factor to distort the Cr-O polyhedral [23]. Taking the positions $^4A_2$ to $^4T_2$ and $^4A_2$ to $^4T_1$ bands, obtained from the optical reflectance spectra (see Fig. 4), and the relationships given by Casalboni et al. [21], $g_{//} = g_e - 8\lambda/\Delta E(^4A_2 \rightarrow {}^4T_2)$, $g_\perp = g_e - 8\lambda/\Delta E(^4A_2 \rightarrow {}^4T_1)$ and $g = (g_{//} + 2\,g_\perp)/3$, where λ is the spin-orbit coupling parameter, we obtained the mean value 1.97 for effective g-factor.

The optical band gap of $YCrO_3$ was determined by using the Kubelka-Munk approach [24,25] in the reflectance spectrum. The relation between the diffuse reflectance of the sample (R_∞), absorption coefficient (K) and scattering coefficient (S) is given by the Kubelka-Munk function $F(R_\infty)$ [25]:

$$F(R_\infty) = (1 - R_\infty)^2/(2R_\infty) = K/S \quad (5)$$

where $R_\infty = R_{sample}/R_{eference}$. The band gap E_g and absorption coefficient α, assuming a direct band gap, are related through the Tauc relation [25]:

$$\alpha h\upsilon = A(h\upsilon - E_g)^{1/2} \quad (6)$$

being ν the photon energy and a proportionality constant. When the powder scatters in a perfectly diffuse manner, the absorption coefficient K becomes equal to 2α. Considering the scattering coefficient S independent of wavelength, and using Eqs. (5) and (6), the following

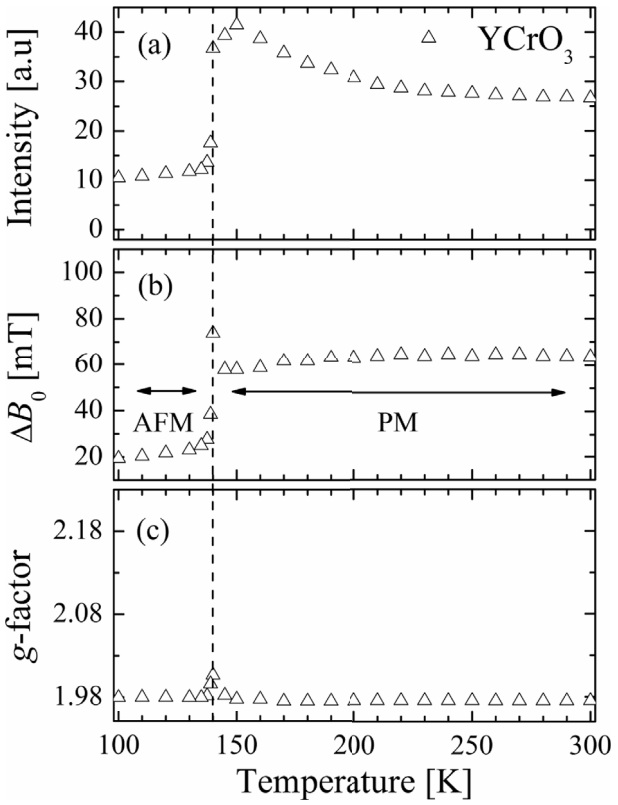

Fig. 5. Temperature dependence of EPR parameters (a) Intensity I_{EPR}, (b) peak-to-peak line width ΔB_0 and (c) *g*-factor for $YCrO_3$. The vertical dotted line shows the temperature where the AFM-PM magnetic transition occurs.

expression can be written:

$$(F(R_\infty)h\upsilon)^2 = A(h\upsilon - E_g)^{1/2} \quad (7)$$

From the plot of $(F(R_\infty)\, h\nu)^2$ versus $h\nu$, inset in Fig. 4, the value of E_g was obtained by extrapolating the linear fitted region to $(F(R_\infty)\, h\nu)^2 = 0$ [25], and its value is 3.72(1) eV, characterizing $YCrO_3$ as a wide band gap material. This value, is comparable to 3.65 eV obtained by Arima et al. [26], measured by optical reflection on optically polished surface of $YCrO_3$ crystals. However, it is greater than the values reported in Refs. [1,20], ranging from 3.03 to 3.24 eV for $YCrO_3$ nanoparticles with size in the range of 32–128 nm. They argued that in nanosized particles the optical band gap scale to the particle size, i.e. the smaller is the nanoparticle the small is the band gap.

3.3. EPR and susceptibility studies

EPR spectra of $YCrO_3$ powder finely crushed were taken in function of the temperature at 9.4 GHz (X–band) are shown in Fig. 5. They are typical of Cr^{3+} ions with $S = 3/2$ occupying sites with rhombic symmetry where the three spins are in the triplet t_{2g} state, and do not display hyperfine structure, as expected for compounds where the chromium ions are magnetically coupled. In the temperature ranges 100–135 K and 150–300 K, the spectra exhibit a single, broad and almost symmetric Lorentzian line shape, and as expected the signal amplitude increases as the temperature decreases. Between 150 and 137 K, the spectra turn very broad, intense and asymmetrical. Fig. 4 shows the intensity I_{EPR} (Fig. 5a) obtained after double integration of the simulated spectra, peak-to-peak line width ΔB_0 (Fig. 5b) and *g*-factor (Fig. 5c) temperature dependency. In the range of 300 to 220 K, the intensity of the spectra exhibits a slight and monotonic increase, when the growth tax increases and reaches a maximum at 150 K, this is in according with expected for paramagnetic system where the EPR spectrum is proportional to the static spin susceptibility [10,27,28]. Below 150 K, the signal intensity presents a small decrease until 140 K following by a pronounced decrease at $T \sim 137$ K remaining almost constant below this temperature, but three times less than that observed at room temperature, leading to a very weak EPR signals. These results can be attributed to decrease of number of paramagnetic centers due the antiparallel spin alignment leading to an antiferromagnetic ordering.

The behavior of the peak-to-peak linewidth ΔB_0 temperature dependence shows in Fig. 5b, reveals that in the PM phase the linewidth is very broad and almost constant within experimental error, with a mean value of ~63 mT, with a maximum value at $T \approx 140$ K, $\Delta B_0 \approx 74$ mT, an indicative that no magnetic fluctuations occur above this temperature, i.e., the magnetic long-range order remains unaltered in the temperature region. Below 140 K, the line width quickly decreases from ~28 mT at 137.5 K until 19.4 mT at 100 K. The observed decrease of ΔB_0 below 140 K is an indication that this compound presents a weak ferromagnetic behavior, as pointed by Alvarez et al. [10]. Fig. 5c shows the dependence of the *g*-factor with the temperature, which are almost constant in the PM phase with $g \sim 1.98(1)$. The PM phase confirms all hypothesis made here about the Cr^{3+} coordination in $YCrO_3$, corroborating the early results and being in good agreement with that found by optical measurements. The *g*-factor value is less than that of free electron (2.0023), is attributed to the changes in the spin-orbit coupling. At 140 K the *g*-factor reached its maximum value, following by a pronounced decrease below 140 K, returning to former value. This behavior of *g*-factor was attributed to an increase in the local magnetic field caused by antiparallel alignment of neighboring spins originated from ferromagnetic interactions. Thus, the Néel temperature T_N determined by means of EPR spectroscopy was 140 K. It is worth mention that in the entire temperature range, our results showed that above and below the Néel temperature the EPR parameters remain almost constant, indicating the presence of a single magnetic phase transition detected by EPR at 140 K. These excluded a possible existence of a second phase transition above T_N due the magnetic fluctuations. It is interesting to note that independent of the method of preparation (see Ref. [9]and [10], for example) at $T_N = 140(2)$ K occurs significant changes in the EPR parameters such as *g*-factor, intensity and line width, that coincides with the temperature phase transition at ~140 K where the magnetic behavior of Cr^{3+} spins change from PM ($T > 140$ K) to AFM phase ($T < 140$ K), with the system exhibiting a weak ferromagnetism, This weak ferromagnetism is because the canting of the Cr^{3+} spins from the antiferromagnetic axis, as expected for this material [11,12,14], and explained by the Dzyaloshinsky-Moriya anisotropic exchange interaction of Cr^{3+}-Cr^{3+} pairs [29,30].

The curve in Fig. 6 shows the dependence of the magnetic susceptibility of $YCrO_3$ with temperature in the interval of 100–300 K, measured with an applied magnetic field of 10 mT. An abrupt increase in the susceptibility values is observed at 140(2) K (see the inset in Fig. 6) denoted as Néel temperature T_N, indicating a weak ferromagnetism with origin in the small canting of the Cr^{3+} spins form the antiferromagnetic (AFM) order, in the AFM G-type magnetic structure [16,31], which could be confirmed by EPR results (Fig. 5). The value of μ_{eff} for Cr^{3+} ion in $YCrO_3$ obtained here is $4.5\mu_B$ is which is in good agreement with those reported in Refs. [32–34], but differs from the theoretical value of $3.87\mu_B$, due to its weak ferromagnetic nature [18], however indicating that Cr^{3+} lies in the high spin configuration, $t_{2g}{}^3$. In addition, in the paramagnetic (PM) phase, above T_N, the χ curve follows the Curie-Weiss law $\chi = C/(T - \Theta)$, where C is the Curie constant related to the effective magnetic moment, μ_{eff}, and Θ is the Curie-Weiss temperature. So, from the fitting of Curie-Weiss law to the χ^{-1} *vs T* graph we have obtained $\Theta = -448$ K, indicating the presence of a strong antiferromagnetic exchange interactions.

In addition, using the molecular field approximation, the relationship between the Curie-Weiss temperature and the exchange interaction *J* (for the Hamiltonian of the Heisenberg type $H_{exc} = -J\mathbf{S}_1\cdot\mathbf{S}_2$) is given

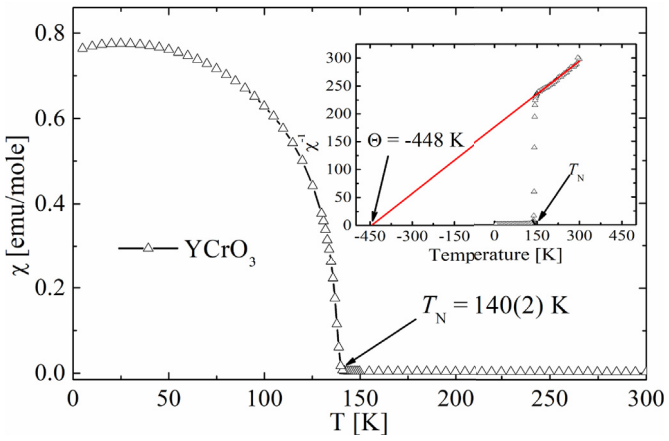

Fig. 6. Temperature variation of magnetic susceptibility for $YCrO_3$. Solid line is only guide for eye. The inset exposes the dependence of the inverse of susceptibility with the temperature, where the solid line represents the linear fit to the Curie-Weiss law.

by $J = -3\Theta/zS(S+1)$ [35], where $z = 6$ is the number of nearest Cr atoms neighbors bridged by O atom (Cr^{3+}-O-Cr^{3+}) and $S = 3/2$ is the Cr^{3+} electronic spin, allow us to $J = -41.5\,cm^{-1}$. This exchange coupling is the main interaction responsible to destroy the fine structure of the Cr^{3+} ions EPR spectrum in the studied compound. Also, the dipolar interaction between neighbor Cr^{3+} ions given by $D_{dip} \approx 3g^2(\mu_B)^2/(2R^3)$, where $R = 3.524$ Å is the shortest Cr^{3+}-Cr^{3+} distance, are calculated, $D_{dip} \sim 0.138\,cm^{-1}$, being much smaller and less important than the exchange interaction that destroys the dipolar broadening, and a single and broad line is observed in the EPR spectra. A careful search in the literature reveals a lot of different values for Curie temperature Θ and consequently different values of the antiferromagnetic interaction. For example, Mall et al. [9] found $\Theta = -431$ K for sample powder prepared by conventional solid-state reaction, Sardar et al. [16] for powder prepared by hydrothermal synthesis found $\Theta = -260$ K and size particle ~1 μm, the same found by Ahmad et al. [36] that used the citrate precursor route to the synthesis and average size particles of 22 nm. Tiwari et al. [33] by conventional solid-state reaction method found $\Theta = -449$ K for sample powders, Durán et al. [37] through combustion reaction method found $\Theta = -325$ K, and Cheng et al. [38] found $\Theta = -239$ K for both single crystal and thin films. The discrepant values of Curie temperatures and the AFM interaction, may be related to the method of sample preparation and on whether the material is ceramics, crystal or powder.

Furthermore, the frustration index for our samples is $f = |\Theta|/T_N = 3.2$, which is an indication that our material is a stable AFM system without magnetic frustration. A material is considered magnetically frustrated if $f > 5$ [39].

4. Conclusions

In this work, we demonstrated that the modified polymeric precursor method is an effective route to prepare single-phase $YCrO_3$ orthochromite with good crystallinity and properties. This method proved to be efficient in producing homogeneous and mono disperse nanoparticles. In addition, we performed a wide and systematic characterization of crystals, improving and confirming some results already published and given new contributions to the understanding of the properties of this material. The diffuse reflectance spectrum exhibited four well defined bands, characteristic of Cr^{3+} ions in distorted octahedral local symmetry, allowing to calculate the crystal field splitting and Racah parameters. The value of $Dq/B = 3.05$ clearly indicates that the Cr^{3+} ions in studied system occupy high crystal field sites. The optical band gap of 3.72(1) eV originated from charge transfer excitations was determinate from diffuse reflectance spectra characterizing this material as an isolator. Also the effective *g*-value calculated from optical and EPR spectroscopy was in good agreement. Finally the EPR parameters measured as function of temperature, made possible to improve the determination of the antiferromagnetic-paramagnetic transition occurring at 140 K, which is attributed to the magnetic short-range spin-spin exchange interaction between pairs of Cr^{3+} ions, $J = -41.5\,cm^{-1}$.

Acknowledgements

This work was supported by CNPq, FAPEG and CAPES. We are grateful to Dra. Carolina Aliaga (Universidad Santiago de Chile, USACH) for part of EPR measurements. We also thanks to LabMic/UFG for providing the SEM images.

References

[1] S. Krishnan, K. Shafakath, R. Philip, N. Kalarikkal, Size dependent nonlinear optical properties of $YCrO_3$ nanosystems, AIP Conf. Proc. 138 (2014) 138–140, https://doi.org/10.1063/1.4862003.
[2] B. Zhang, Q. Zhao, A. Chang, Y. Liu, Y. Li, Y. Wu, Synthesis of $YCrO_3$ ceramics through a field-assisted sintering technique, J. Mater. Sci. Mater. Electron. 25 (2014) 1400–1403, https://doi.org/10.1007/s10854-014-1741-5.
[3] J.T. Looby, L. Katz, Yttrium chromium oxide, A new compound of the perowskite type, J. Am. Chem. Soc. 76 (1954) 6029–6030, https://doi.org/10.1021/ja01652a047.
[4] L. Katz, On the unit cell of $YCrO_3$, Acta Crystallogr. 8 (1955) 121–122, https://doi.org/10.1107/S0365110X55000522.
[5] S. Geller, E.A. Wood, Crystallographic studies of perovskite-like compounds. I. Rare earth orthoferrites and $YFeO_3$, $YCrO_3$, $YAlO_3$, Acta Crystallogr. 9 (1956) 563–568, https://doi.org/10.1107/S0365110X56001571.
[6] C.R. Serrao, A.K. Kundu, S.B. Krupanidhi, U.V. Waghmare, C.N.R. Rao, Biferroic $YCrO_3$, Phys. Rev. B 72 (2005) 2–5, https://doi.org/10.1103/PhysRevB.72.220101.
[7] K. Ramesha, A. Llobet, T. Proffen, C.R. Serrao, C.N.R. Rao, Observation of local non-centrosymmetry in weakly biferroic $YCrO_3$, J. Phys. Condens. Matter 19 (2007) 102202, https://doi.org/10.1088/0953-8984/19/10/102202.
[8] V.M. Jüdin, A.B. Sherman, Weak ferromagnetism of $YCrO_3$, Solid State Commun. 4 (1966) 661–663, https://doi.org/10.1016/0038-1098(66)90067-6.
[9] A.K. Mall, A. Dixit, A. Garg, R. Gupta, Temperature dependent electron paramagnetic resonance study on magnetoelectric $YCrO_3$, J. Phys. Condens. Matter 29 (2017) 495805, https://doi.org/10.1088/1361-648X/aa97bc.
[10] G. Alvarez, M.P. Cruz, A.C. Durán, H. Montiel, R. Zamorano, Weak ferromagnetism in the magnetoelectric detected by microwave power absorption measurements, Solid State Commun. 150 (2010) 1597–1600, https://doi.org/10.1016/j.ssc.2010.06.047.
[11] V. Bedekar, R. Shukla, A.K. Tyagi, Nanocrystalline $YCrO_3$ with onion-like structure and unusual magnetic behaviour, Nanotechnology 18 (2007) 155706, https://doi.org/10.1088/0957-4484/18/15/155706.
[12] G. Cruciani, M. Ardit, M. Dondi, F. Matteucci, M. Blosi, M.C. Dalconi, S. Albonetti, Structural relaxation around Cr^{3+} in $YAlO_3$-$YCrO_3$ perovskites from electron absorption spectra, J. Phys. Chem. A 113 (2009) 13772–13778, https://doi.org/10.1021/jp9043072.
[13] R.S. Pavlov, V.B. Marzá, J.B. Carda, Electronic absorption spectroscopy and colour of chromium-doped solids, J. Mater. Chem. 12 (2002) 2825–2832, https://doi.org/10.1039/b201802k.
[14] T. Tachiwaki, Y. Kunifusa, M. Yoshinaka, K. Hirota, Formation, powder characterization and sintering of $YCrO_3$ prepared by a sol – gel technique using hydrazine, Int. J. Inorg. Mater. 3 (2001) 107–111.
[15] S. Krishnan, N. Kalarikkal, Synthesis of $YCrO_3$ nanoparticles through PAA assisted sol-gel route, J. Sol. Gel Sci. Technol. 66 (2013) 6–14, https://doi.org/10.1007/s10971-013-2959-z.
[16] K. Sardar, M.R. Lees, R.J. Kashtiban, J. Sloan, R.I. Walton, Direct hydrothermal synthesis and physical properties of rare-earth and yttrium orthochromite perovskites, Chem. Mater. 23 (2011) 48–56, https://doi.org/10.1021/cm102925z.
[17] J.F. Carvalho, F.S. De Vicente, S. Pairis, P. Odier, A.C. Hernandes, A. Ibanez, Synthesis of YAP nanopowder by a soft chemistry route, J. Eur. Ceram. Soc. 29 (2009) 2511–2515, https://doi.org/10.1016/j.jeurceramsoc.2009.03.005.
[18] G.V. Subba Rao, C.N.R. Rao, J.R. Ferraro, Infrared and electronic spectra of rare earth perovskites. ortho-chromites, -manganites and -ferrites, Appl. Spectrosc. 24 (1970) 436–444, https://doi.org/10.1366/000370270774371426.
[19] D.S. Patil, N. Venkatramani, V.K. Rohatgi, Infrared spectra of the ceramic $YCrO_3$ doped with strontium, J. Mater. Sci. Lett. 7 (1988) 413–414, https://doi.org/10.1007/BF01730761.
[20] S. Krishnan, C.S. Suchand Sandeep, R. Philip, N. Kalarikkal, Two-photon assisted excited state absorption in multiferroic $YCrO_3$ nanoparticles, Chem. Phys. Lett. 529 (2012) 59–63, https://doi.org/10.1016/j.cplett.2012.01.047.
[21] M. Casalboni, V. Ciafardone, G. Giuli, B. Izzi, E. Paris, P. Prosposito, An optical study of silicate glass containing Cr^{3+} and Cr^{6+} ions, J. Phys. Condens. Matter 8 (1996) 9059–9069, https://doi.org/10.1088/0953-8984/8/46/011.
[22] F. Rasheed, K. O'Donnell, B. Henderson, D. Hollis, Disorder and the optical

spectroscopy of Cr^{3+}-doped glasses: I. Silicate glasses, J. Phys. Condens. Matter 3 (1991) 1915–1930, https://doi.org/10.1088/0953-8984/3/12/022.
[23] P.S. Devi, Citrate gel processing of the perovskite lanthanide chromites, J. Mater. Chem. 3 (1993) 373, https://doi.org/10.1039/jm9930300373.
[24] P. Kubelka, F. Munk, Ein Beitrag zur Optik der Farbanstriche, Zeitschrift Für Tech. Phys. 12 (1931) 593–601.
[25] S. Som, S.K. Sharma, T. Shripathi, Influences of doping and annealing on the structural and photoluminescence properties of Y2O3 nanophosphors, J. Fluoresc. 23 (2013) 439–450, https://doi.org/10.1007/s10895-013-1160-7.
[26] T. Arima, Y. Tokura, J.B. Torrance, Variation of optical gaps in perovskite-type 3d transition-metal oxides, Phys. Rev. B 48 (1993) 17006–17009, https://doi.org/10.1103/PhysRevB.48.17006.
[27] J.A. Weil, J.R. Bolton, Electron Paramagnetic Resonance: Elementary Theory and Practical Applications, second ed., John Wiley & Sons, Inc, Publications, New Jersey, USA, New Jersey, 2007, https://doi.org/10.1002/0470084987.
[28] J.R. Pilbrow, Transition Ion Electron Paramagnetic Resonance, Clarendon Press, Oxford, 1980.
[29] I. Dzyaloshinsky, A thermodynamic theory of "weak" ferromagnetism of antiferromagnetics, J. Phys. Chem. Solid. 4 (1958) 241–255, https://doi.org/10.1016/0022-3697(58)90076-3.
[30] T. Moriya, Anisotropic superexchange interaction and weak ferromagnetism, Phys. Rev. 120 (1960) 91–98, https://doi.org/10.1103/PhysRev.120.91.
[31] I.S. Jacobs, H.F. Burne, L.M. Levinson, Field-induced spin reorientation in $YFeO_3$ and $YCrO_3$, J. Appl. Phys. 42 (1971) 1631–1632, https://doi.org/10.1063/1.1660372.
[32] J. Prado-Gonjal, R. Schmidt, J.J. Romero, D. Ávila, U. Amador, E. Morán, Microwave-assisted synthesis, microstructure, and physical properties of rare-earth chromites, Inorg. Chem. 52 (2013) 313–320, https://doi.org/10.1021/ic302000j.
[33] B. Tiwari, M.K. Surendra, M.S.R. Rao, HoCrO3 and YCrO3 : a comparative study, J. Phys. Condens. Matter 25 (2013) 216004, https://doi.org/10.1088/0953-8984/25/21/216004.
[34] J. Prado-Gonjal, E. Morán, Síntesis asistida por microondas de sólidos inorgánicos, An. Quím 107 (2011) 129–136.
[35] O. Kahn, Molecular Magnetism, Wiley, VCH, U.S.A, 1993.
[36] T. Ahmad, I.H. Lone, Citrate precursor synthesis and multifunctional properties of $YCrO_3$ nanoparticles, N. J. Chem. 40 (2016) 3216–3224, https://doi.org/10.1039/C5NJ02763B.
[37] A. Durn, A.M. Arvalo-Lpez, E. Castillo-Martnez, M. Garca-Guaderrama, E. Moran, M.P. Cruz, F. Fernndez, M.A. Alario-Franco, Magneto-thermal and dielectric properties of biferroic $YCrO_3$ prepared by combustion synthesis, J. Solid State Chem. 183 (2010) 1863–1871, https://doi.org/10.1016/j.jssc.2010.06.001.
[38] Z.X. Cheng, X.L. Wang, S.X. Dou, H. Kimura, K. Ozawa, A novel multiferroic system: rare earth chromates, J. Appl. Phys. 107 (2010) 2010–2012, https://doi.org/10.1063/1.3360358.
[39] R. Moessner, Magnets with strong geometric frustration, Can. J. Phys. 79 (2001) 1283–1294, https://doi.org/10.1139/p01-123.